Communication: First-principles evaluation of alkali ion adsorption and ion exchange in pure silica LTA zeolite

Vancho Kocevski, Benjamin D. Zeidman, Charles H. Henager, and Theodore M. Besmann

Citation: The Journal of Chemical Physics **149**, 131102 (2018); doi: 10.1063/1.5051347
View online: https://doi.org/10.1063/1.5051347
View Table of Contents: http://aip.scitation.org/toc/jcp/149/13
Published by the American Institute of Physics

Communication: First-principles evaluation of alkali ion adsorption and ion exchange in pure silica LTA zeolite

Vancho Kocevski,[1,a)] Benjamin D. Zeidman,[2] Charles H. Henager, Jr.,[2] and Theodore M. Besmann[1]
[1]*Nuclear Engineering Program, University of South Carolina, Columbia, South Carolina 29208, USA*
[2]*Pacific Northwest National Laboratory, P.O. Box 999, Richland, Washington 99352, USA*

(Received 7 August 2018; accepted 26 September 2018; published online 4 October 2018)

Using first-principles calculations, we studied the adsorption of alkali ions in pure silica Linde Type A (LTA) zeolite. The probability of adsorbing alkali ions from solution and the driving force for ion exchange between Na^+ and other alkali ions at the different adsorption sites were analyzed. From the calculated ion exchange isotherms, we show that it is possible to exchange Na^+ with K^+ and Rb^+ in water, but that is not the case for systems in a vacuum. We also demonstrate that a solvation model should be used for the accurate representation of ion exchange in an LTA and that dispersion interactions should be introduced with care. *Published by AIP Publishing.* https://doi.org/10.1063/1.5051347

With their microporous structure, ease of fabrication, and diversity of structural types, zeolites have become a leading material for adsorbents, molecular sieves, catalysts, membranes, etc. Recently, particular interest has been directed toward the Linde Type A (LTA) zeolite, especially because of its very high exchange capacity and excellent cation exchange properties.[1] The easily exchangeable Na^+ ions make the LTA zeolite very useful for various applications, such as sorbents,[2] enhancing detergent efficiency,[3] desalination,[4] or cleaning wastewater.[5–7] These properties of zeolites are also applied to capturing radioisotopes, such as Cs and Sr, from nuclear waste streams.[7,8] Our interest is in nuclear waste forms, utilizing the ion exchange capability of LTA to exchange Na^+ ions with larger alkali ions, specifically Cs^+.

In addition to the growing number of experimental studies on zeolites, there are many modeling studies detailing the application of various computational methods in studying the different properties of zeolites. Such modeling is very useful for complementing experimental findings by improving the fundamental understanding of the studied systems or predicting new materials and properties. Because of the large size of the LTA, there have been very few computational studies of this system.[9,10] Unique to our efforts is using density functional theory (DFT) to calculate the energies for alkali ions adsorbing in LTAs and to obtain the driving force for exchanging Na^+ ions with other alkali ions. Furthermore, we provide a detailed assessment of the validity of different models, i.e., systems in vacuum or in water, and whether the use of dispersion interactions in representing ion exchange in an LTA is necessary. Subsequently the application of this study to more complex nuclear waste forms, such as Prussian blue analogs, that have the potentially to effectively immobilize nuclear waste elements will be considered.

The LTA is an aluminosilicate zeolite with the Si/Al ratio of 1 and the formula $Na_{12}[(AlO_2)_{12}(SiO_2)_{12}]\cdot xH_2O$ and has a high number of adsorption (exchange) sites. It has a cubic framework, comprised of 3D interconnected β-cages [Fig. 1(b)] that are connected to four-member rings giving rise to α-cages [Figs. 1(a) and 1(c)]. The α-cages are interconnected in 3D by 8-membered apertures [Fig. 1(a), site 3] forming the pore system in the LTA. The unit cell has three unique adsorption sites, with site diameters of 4.4 Å, 3.6 Å, and 6.9 Å for sites 1, 2, and 3, respectively [see Figs. 1(a) and 1(b)]. Besides the high Al content LTA, a pure silica LTA (ps-LTA) has also been synthesized using an organic structure-directing agent obtained by self-assembly.[11] Note that in our study, we are using the ps-LTA because the very large size of the aluminosilicate LTA (640 atoms) makes it prohibitive to perform DFT calculations within a reasonable timeframe.

The DFT calculations were performed using the Vienna *Ab initio* Simulation Package (VASP),[12,13] using the projector augmented plane wave (PAW) method[14,15] and the Perdew-Burke-Ernzerhof (PBE) generalised-gradient approximation.[16] To account for the dispersion interactions, we considered Van der Waals (VdW) corrections as per the DFT-D3 method.[17] We used a $3 \times 3 \times 3$ k-point mesh, 520 eV cutoff energy for the planewave basis set, and 10^{-8} eV and 0.001 Å/eV energy and forces convergence criteria, respectively. The volume and ionic positions within each of the structures were relaxed, while the cubic framework was kept constant. We calculated the phonon spectra of the ps-LTA using the phonopy code[18] to evaluate the stability of ps-LTA. As noted in Fig. S1 of the supplementary material, the absence of negative phonon frequencies confirmed that ps-LTA is dynamically stable and, thus, has not relaxed to a transition state. Because ion exchange in zeolites happens in aqueous solutions, we also considered the systems to be surrounded by water, employing the implicit solvation model VASPsol.[19,20] The solvent model introduced in VASPsol assumes a quantum-mechanical

a)Author to whom correspondence should be addressed: kocevski@mailbox.sc.edu and vancho.vk@gmail.com.

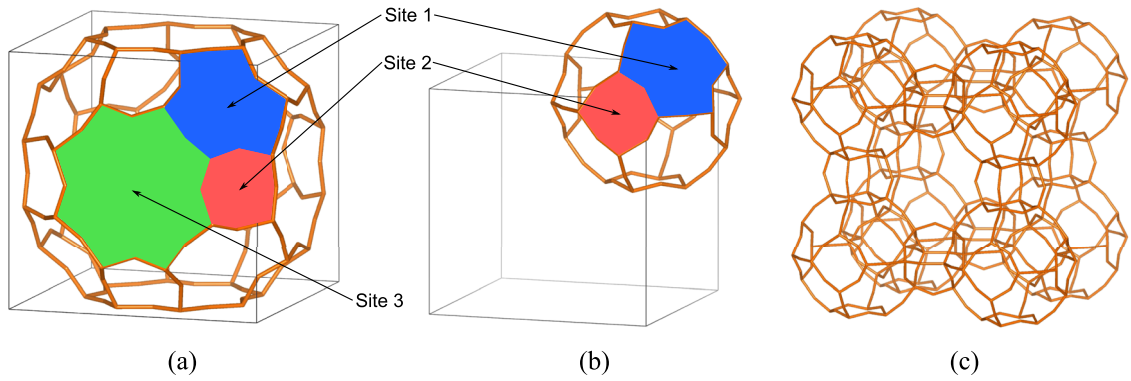

FIG. 1. Representation of (a) α-cage, (b) β-cage, and (c) α-cage (middle) with 8 surrounding β-cages of LTA. The adsorption sites 1, 2, and 3 are shown in blue, red, and green, respectively.

solute in a cavity surrounded by a continuum of solvents, and it has been parameterized for solvation energies of various molecules in water and reaction barriers.[20] Despite the parameterization for molecules in water, it has been shown that VASPsol reproduces well the trends in charged systems, such as charging curves,[21] and alkali ion adsorption on Pt surfaces.[22]

Using first-principles calculations, the adsorption energy of a single ion A^+, $E^{A}_{ads,0}$, can be calculated by the general equation

$$\boldsymbol{E^{A}_{ads,0}} = \boldsymbol{E(LTA : A) - E(LTA) - \mu^{0}_{A}}, \quad (1)$$

where E(LTA) and E(LTA:A) are the DFT calculated total energies of the ps-LTA and ps-LTA with adsorbed alkali ion, A^+, respectively, and μ^0_A is the standard chemical potential of A^+. For systems in vacuum, μ^0_A is the DFT calculated total energy of a single ion, and for systems in aqueous solution, the μ^0_A was calculated using the method proposed by Persson *et al.*[23] (see the supplementary material for more details). Shown in Fig. 2 are the calculated $E^{A}_{ads,0}$ for A = Na^+, K^+, Rb^+, and Cs^+, using the PBE and DFT-D3 methods, in vacuum and in water. The results for the adsorption on site 2 are not shown in Fig. 2 because the ions relaxed to site 1 from initial positions on site 2, except for Na^+ calculated using PBE and DFT-D3 and K^+ calculated using PBE, which relaxed to site 2.

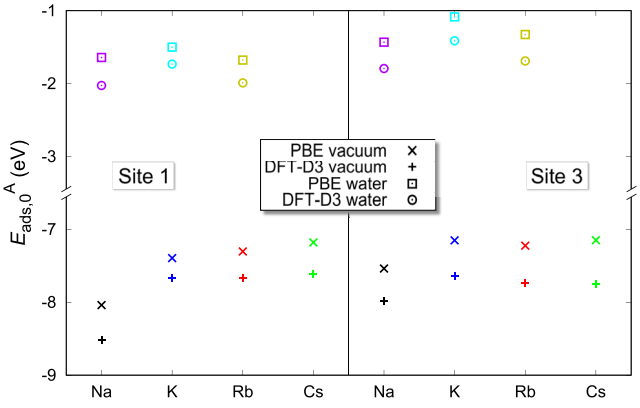

FIG. 2. Adsorption energies, $\boldsymbol{E^{A}_{ads,0}}$, of Na^+ (black), K^+ (blue), Rb^+ (red), and Cs^+ (green) in vacuum and Na^+ (purple), K^+ (cyan), and Rb^+ (yellow) in water, at the site 1 and site 3 in ps-LTA, calculated with the PBE and DFT-D3 methods.

Evidently, a Na^+ ion on both site 1 and site 3 has the lowest adsorption energy, i.e., is the preferable ion, compared to K^+, Rb^+, and Cs^+. When DFT-D3 is used, the $E^{A}_{ads,0}$ becomes more negative compared to those calculated using only PBE. The inclusion of dispersion interactions by DFT-D3 will increase the computed bond strength between the ions and ps-LTA, and consequently the energy of the system will become more negative, which explains the difference in $E^{A}_{ads,0}$ values. Once the systems are considered to be in water, both $E^{A}_{ads,0}$ values become more positive and differences between values diminish, especially between the Na^+ and the other ions, with the Rb^+ becoming the preferred ion on site 1. This difference in $E^{A}_{ads,0}$ is mainly due to the formation of alkali ions in vacuum, which is energetically costly, especially Na^+ whose ionization energy leads highly positive standard chemical potentials. Whereas, aqueous ions have negative standard chemical potentials, with very small variations between species (see Table S1). we have no results for systems for Cs^+ in water because of convergence issues with the solvation model.

In its current form, Eq. (1) does not take into account the change in the chemical potential due to changes in ion concentration in water. To consider this, Eq. (1) can be rewritten as

$$E^{A}_{ads} = E(LTA : A) - E(LTA) - \mu_A = E^{A}_{ads,0} - k_b T \ln(x_A \gamma_A), \quad (2)$$

$$\mu_A = \mu^0_A + k_b T \ln(x_A \gamma_A), \quad (3)$$

where μ_A, x_A, and γ_A are the chemical potential, mole fraction, and activity coefficient of ion A^+ in water, respectively, k_b is the Boltzmann constant, and T is the thermodynamic temperature. Thus, E^{A}_{ads} can now be calculated as a function of the mole fraction of A^+. Moreover, considering ion concentration allows the determination of the mole fraction ratio at which ion A_1 becomes preferred over ion A_2, on a specific adsorption site. This can be found by defining the adsorption energy difference, ΔE_{ads}, for A_1 and A_2 ions as

$$\Delta E_{ads} = E^{A_1}_{ads} - E^{A_2}_{ads} = E^{A_1}_{ads,0} - E^{A_2}_{ads,0} - k_b T \ln\left(\frac{x_{A_1}\gamma_{A_1}}{x_{A_2}\gamma_{A_2}}\right). \quad (4)$$

Shown in Fig. 3 is the ΔE_{ads} as a function of the mole fraction ratio, x_A/x_{Na}, between A^+ (A_1) and Na^+ (A_2) ions on sites 1 and 3 (A = K, Rb, Cs), for ps-LTA in vacuum and in water, calculated using PBE and DFT-D3. The negative ΔE_{ads}, a region in Fig. 3, is the x_A/x_{Na} range over which the A^+ ion is preferred over the Na^+ ion. The γ_A values were calculated using parameters obtained by fitting experimental data reported by Kielland[24] to the Debye-Hückel equation, as detailed in the supplementary material.

Clearly, the smaller the difference between the $E^A_{ads,0}$ of A^+ and Na^+, the smaller the x_A/x_{Na} ratio at which the ion A^+ will replace Na^+. The difference between x_A/x_{Na} at which A^+ is replacing Na^+ (the points at $\Delta E_{ads} = 0$ eV) for the two sites becomes smaller when the systems are considered to be in water. Unlike ions in vacuum, for ions in water, site 1 becomes the favorable site, which agrees with observations in synthesized LTA, in which Na^+ ions occupy each of the eight site 1 positions.[1] Thus, ΔE_{ads} as a function of the mole fraction ratio provides useful information on the competing driving forces for adsorbing two solution ions on the zeolite. As zeolites are readily used for ion exchange, calculating the energy, i.e., the driving force for ion exchange, can allow the prediction of behavior. Using Eq. (2), the ion exchange energy, ΔE_{ie}, can be defined as

$$\begin{aligned}\Delta E_{ie} &= E^{A_1}_{ads} - E^{A_2}_{ads} \\ &= E(\text{LTA} : A_1) - E(\text{LTA} : A_2) - \mu_{A_1} + \mu_{A_2}, \end{aligned} \quad (5)$$

where $\mu_{A_2} - \mu_{A_1}$ is the A_2 and A_1 ions' chemical potential difference. A positive ion exchange energy indicates the preferred adsorption of A_2 over A_1, where A_1 is the preferred ion if the ion exchange energy is negative. When $\Delta E_{ie} = 0$ eV, the following ion exchange reaction will be at equilibrium:

$$A_1(aq) + A_2(zeo) = A_1(zeo) + A_2(aq), \quad (6)$$

where (aq) or (zeo) indicates that the ions are in aqueous solution or adsorbed on the zeolite, respectively. Using Eq. (5), one can identify the chemical potential regions where Na^+ ions exchange with $A^+ = K^+$, Rb^+, and Cs^+ by plotting the ion chemical potentials at which Eq. (6) is satisfied. Shown in Fig. S2 of the supplementary material are the chemical potential regions for exchanging Na^+ with A^+ at the two sites, calculated using PBE and DFT-D3, in water and in vacuum, where the area below the lines depict the Na^+ rich region.

Relative chemical potentials would be very useful if they could be easily evaluated, which is not the case. From the ion exchange reaction, Eq. (6), it follows that the chemical potential of ion A^+, μ_A, is defined by the difference in the chemical potential of an ion in aqueous solution, μ^{aq}_A, and in the zeolite, μ^{zeo}_A, i.e., $\mu_A = \mu^{aq}_A - \mu^{zeo}_A$. For ions in aqueous solution, a quantity that can be easily measured and manipulated is the mole fraction, x, as shown by Eq. (3). For ions in a zeolite, Adamson and Gast[25] have shown using statistical thermodynamics that the μ^{zeo}_A can be described as

$$\mu^{zeo}_A = k_b T \ln\left(\frac{\theta^i_A}{1-\theta^i_A}\right) - k_b T \ln\left[Q^i_A(T)\right], \quad (7)$$

where θ^i_A is the fraction of the exchanged sites i, occupied by the ion, A, and Q^i_A is the partition function of the adsorbed ion A on site i.

Introducing Eqs. (3) and (7) into Eq. (5), the ion exchange energy for the reaction of Eq. (6) can be rewritten as

$$\begin{aligned}\Delta E_{ie} = E^{A_1}_{ads,0} - E^{A_2}_{ads,0} - k_b T \ln\left(\frac{x_{A_1}\gamma_{A_1}}{x_{A_2}\gamma_{A_2}}\right) \\ + k_b T \ln\left(\frac{\theta^i_{A_1}(1-\theta^i_{A_2})}{(1-\theta^i_{A_1})\theta^i_{A_2}}\right) - k_b T \ln\left(\frac{Q^i_{A_1}}{Q^i_{A_2}}\right). \end{aligned} \quad (8)$$

This means that ΔE_{ie} can now be calculated as a function of mole fraction of the exchanging ions (x_{A_1}, x_{A_2}) and the fraction of ions on site i in the zeolite ($\theta^i_{A_1}, \theta^i_{A_2}$). Using this definition of ΔE_{ie}, we can now plot the ion mole fraction in solution, $X^{sol}_{A_1}$, and that on site i of the zeolite, $X^i_{A_1}$, with which the A^+ ion will exchange with Na^+. To do that, however, we first need to rewrite Eq. (8) at $\Delta E_{ie} = 0$ with $\theta^i_{A_2} = 1 - \theta^i_{A_1}$, $x_{A_2} = 1 - x_{A_1}$,

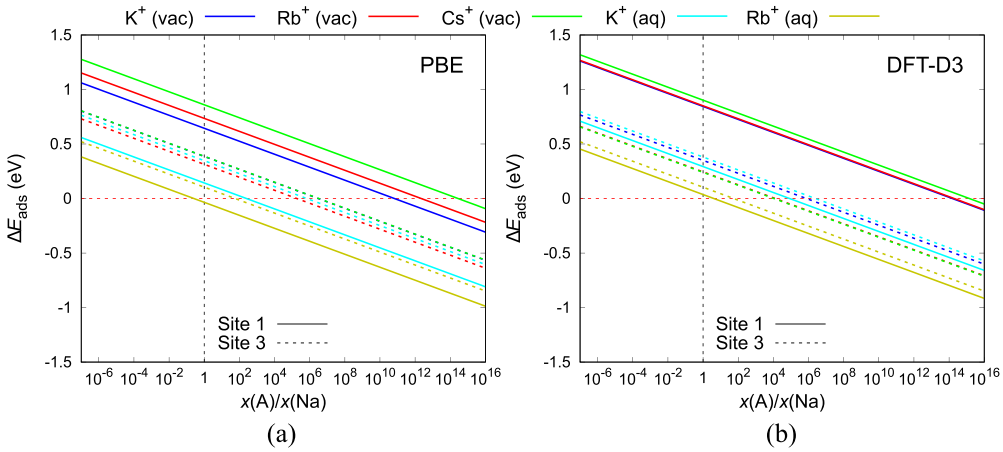

FIG. 3. Adsorption energy difference, ΔE_{ads}, on site 1 (solid line) and 3 (dashed line) as a function of the mole fraction ratio, x_A/x_{Na}, between A = K^+, Rb^+, and Cs^+ ions and Na^+ ion, calculated using (a) PBE and (b) DFT-D3. The Na^+/K^+, Na^+/Rb^+, and Na^+/Cs^+ isotherms in vacuum (vac) are shown in blue, red, and green, respectively, and Na^+/K^+ and Na^+/Rb^+ isotherms in water (aq) are shown in cyan and yellow, respectively.

and $X^{\text{sol}} = X^{\text{sol}}_{\text{A}_1}/1 - X^{\text{sol}}_{\text{A}_1}$, obtaining

$$X^{i}_{\text{A}_1} = \frac{\sqrt{aX^{\text{sol}}}}{1+\sqrt{aX^{\text{sol}}}}, a = e^{\frac{-\Delta E^{0}_{\text{ads}}}{k_b T}} \frac{Q^{i}_{\text{A}_1}}{Q^{i}_{\text{A}_2}} \frac{\gamma_{\text{A}_1}}{\gamma_{\text{A}_2}}, \qquad (9)$$

$$\Delta E^{0}_{\text{ads}} = E^{\text{A}_1}_{\text{ads},0} - E^{\text{A}_2}_{\text{ads},0}.$$

By defining the temperature, T, and the standard molality of the solution, x_0, we can now plot ion exchange isotherms. Shown in Fig. 4 are the PBE and DFT-D3 calculated isotherms for exchanging Na^+ with $A^+ = K^+$, Rb^+, and Cs^+ on site 1 and 3, at $T = 300$ K, and $x_0 = 0.1$M, for ps-LTA in vacuum and in water. Note that for calculating the partition function ratio in Eq. (9), we only considered the translational, rotational, and electronic contributions. We omitted the vibrational contribution because one needs to calculate the phonons to obtain this term, and considering the number of systems and their size, the computational cost of such DFT phonon calculations for such large systems was not reasonable.

From the isotherms in Fig. 4, it is evident that there is only one case where complete exchange is possible, Fig. 4(a) (solid yellow line), depicted by the sigmoidal isotherm. There are 10 cases where only partial ion exchange is achieved, and in the rest of the cases, 9 in total, ion exchange is not possible. Both, PBE and DFT-D3 in vacuum predict that Na^+ ions can only be partially exchanged or cannot be exchanged at all with K^+, Rb^+, or Cs^+ at any of the sites, which comes from the very negative $E^{\text{A}}_{\text{ads},0}$ values for Na^+. For systems in water, PBE shows complete exchange of Na^+ with Rb^+ on site 1 and partial exchange on site 3, while DFT-D3 shows only partial exchange on sites 1 and 3. In water, a partial K^+/Na^+ exchange on site 1 is predicted by both PBE and DFT-D3, with a very small fraction of partial exchange on site 3. Also, Cs^+/Na^+ partial exchange is shown by DFT-D3 as possible in vacuum on site 3. Although we do not have results for Cs^+/Na^+ exchange in water, there is a clear trend of increasing exchange with increasing ion size. Thus, we expect that Na^+ ions are exchanged with Cs^+ ions, which could make the ps-LTA useful for concentrating Cs radioisotope waste streams.

To understand the performance of DFT in accurately representing the adsorption of alkali ions on the ps-LTA, a detailed look at the different adsorption sites is necessary. Because of the different ion sizes, the interaction of the ions with the diverse sizes and shapes of the sites will vary. Site 2 is the smallest, where each of the adsorbed ions is bonded to only two oxygen atoms from the framework (see Fig. S3). Having a small number of ion–oxygen (A–O) bonds, and an increasing bond length with increasing ion size, means that the larger the ions, the weaker the bonding at the site, allowing for the ions to easily move; this is the case for all of the ions tested here, except Na^+. Indeed, the Na^+ ion bonds strongly to the site 2, while the other three alkali ions migrate to site 1 during the relaxation of the structures. The middle-sized site 1 is the preferred site for the Na^+ ion, which arises from the strong bonding between the Na^+ and the O atoms, seen in the shorter Na–O bond lengths (see Table S3 of the supplementary material). The preference of Na^+ for site 1, indicated by the significantly lower adsorption energy, explains why we do not predict exchange with Na^+ on site 1 in vacuum.

When dispersion interactions are considered, it is observed that the bonding between the Na^+ and site 1 is increased compared to the other ions, demonstrated by the decrease in A–O bond length and a more negative adsorption energy with respect to the other ions. In addition, during the relaxation of the structures, the K^+ ion moved from site 2 to site 1 when dispersion interactions were included, which was not the case when only PBE was used. The K^+ ion thus moved to an adsorption site with a larger number of K–O bonds; site 1 has three K–O bonds, hence a site with stronger interaction with the K^+. This movement of K^+ toward the adsorption site with stronger interaction can be attributed to the induced stronger bonding when dispersion interactions are included. Therefore, when studying the adsorption of ions on zeolites, dispersion interactions should be introduced with caution, being mindful of the bonding strength between the ions and adsorption sites.

Unlike the case for Na^+, the adsorption energies of the K^+, Rb^+, and Cs^+ ions in vacuum are lower for site 3 than for site 1, which can be explained by examining the bonding between the ions and the O atoms of the site. When adsorbed on site 3, the ions are bonded to four O atoms (see Fig. S3), except for Na^+, while on site 1, they are bonded to three O atoms. Furthermore, the ions on site 3 are in planar coordination, unlike the ions on site 1 that are above the O atoms plane. Increasing ion size causes increased A–O bond length, causing the O–A–O bond angles for the ions on site 1 to decrease (<90°), while the O–A–O bond angles on site 3 are unchanged

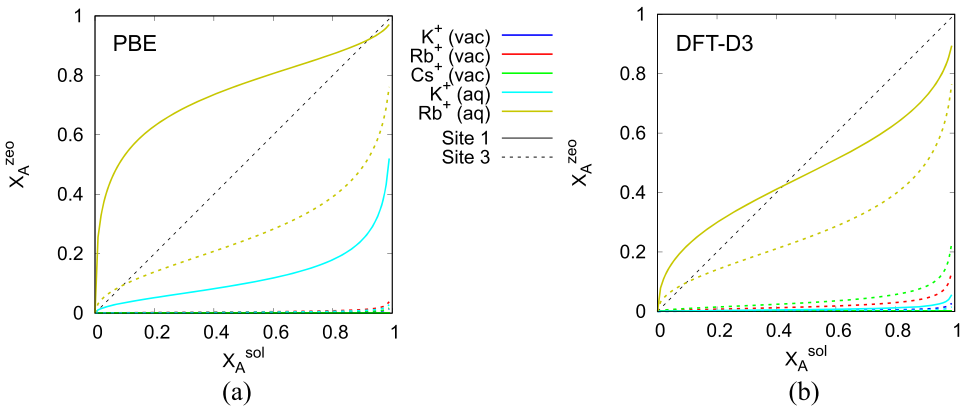

FIG. 4. Ion exchange isotherms for Na^+ with A = K^+, Rb^+, and Cs^+, on site 1 (solid line) and 3 (dashed line), at 0.1M and 300 K, calculated using (a) PBE and (b) DFT-D3. The Na^+/K^+, Na^+/Rb^+, and Na^+/Cs^+ isotherms in vacuum (vac) are shown in blue, red, and green, respectively, and Na^+/K^+ and Na^+/Rb^+ isotherms in water (aq) are shown in cyan and yellow, respectively.

(90°), except for O–Na–O bond angles (see Table S3). A larger number of A–O bonds give rise to more negative potential energy for the systems, whereas the decrease in O–A–O bond angles has an opposite effect, increasing the potential energy. The combination of these effects, increased number of A–O bonds, and constant O–A–O bond angles explains why the K^+, Rb^+, and Cs^+ ions in vacuum prefer site 3 over site 1. However, unlike the ions on site 3 because the ions on site 1 are above the O atoms plane, they can be surrounded by water. This influences the ion–oxygen bond strength, and site 1 becomes the dominant site for these ions in aqueous solution, which is experimentally observed. Thus, to accurately represent these systems using DFT calculations requires the use of a solvation model.

We presented a detailed study of the adsorption of alkali ions on ps-LTA and the exchange of Na^+ ions with other larger alkali ions. We also investigated how ion exchange in ps-LTA is influenced by the surrounding medium, vacuum, or solvent and by the introduction of dispersion interactions. For systems where stronger interactions between the ion and the adsorption site occur, in our case for Na^+ on site 1, dispersion interactions may introduce stronger bonding with more negative system potential energy. This will cause the adsorption energy of the ion to be significantly more negative compared to the adsorption energy of other less strongly bonded ions, leading to predicting exchange of Na^+ on site 1 for other ions to be impossible. In water, the adsorption energies of the different ions are more similar, indicating a weakening of the dispersion interactions. An increase in the adsorption energies in water calculated using only PBE is also observed. The similarity in adsorption energies gives rise to the probability of partially exchanging Na^+ for larger alkali ions at each of the sites, with complete Rb^+/Na^+ exchange being possible on site 1, as shown by PBE. In general, considering the systems to be in water gives a more accurate representation of the ion–zeolite interaction, regardless whether dispersion interactions are used.

See supplementary material for complete information on the ions' activity coefficient and chemical potentials, as well as the bonding at adsorption site details, and chemical potential region results.

This work is supported by the U.S. Department of Energy, Office of Science, Basic Energy Sciences, under Award No. DE-SC0016575 (Center for Hierarchical Waste Form Materials). This research used computational resources provided by the National Energy Research Scientific Computing Center (NERSC) and the HPC cluster Hyperion, supported by The Division of Information Technology at the University of South Carolina.

[1] D. W. Breck, W. G. Eversole, R. M. Multon, T. B. Reed, and T. L. Thomas, J. Am. Chem. Soc. **78**, 5963 (1956).
[2] O. Cheung and N. Hedin, RSC Adv. **4**, 14480 (2014).
[3] R. P. Townsend and E. N. Coker, Stud. Surf. Sci. Catal. **137**, 467 (2001).
[4] E. I. Basaldella, P. G. Vázquez, F. Iucolano, and D. Caputo, J. Colloid Interface Sci. **313**, 574 (2007).
[5] Y. Petit de Pena and W. Rondon, Am. J. Anal. Chem. **4**, 387 (2013).
[6] A. Malekpour, A. Samadi-Maybodi, and M. R. Sadati, Braz. J. Chem. Eng. **28**, 669 (2011).
[7] H. Nakamura, M. Okumura, and M. Machida, J. Phys. Soc. Jpn. **82**, 023801 (2013).
[8] B. Said, A. Grandjean, Y. Barre, F. Tancret, F. Fajula, and A. Galarneau, Microporous Mesoporous Mater. **232**, 39 (2016).
[9] C. E. Hernandez-Tamaro, A. Roldan, P. E. Ngoepe, and N. H. de Leeuw, J. Chem. Phys. **147**, 074701 (2017).
[10] R. E. Salmas, B. Demir, E. Yildirim, A. Sikecioğlu, M. Yurtsever, and M. G. Ahunbay, J. Phys. Chem. C **117**, 1663 (2013).
[11] A. Corma, F. Rey, J. Ruis, M. J. Sabater, and S. Valencis, Nature **431**, 287 (2004).
[12] G. Kresse and J. Furthmüller, Phys. Rev. B **54**, 11169 (1996).
[13] G. Kresse and J. Furthmüller, Comput. Mater. Sci. **6**, 15 (1996).
[14] P. E. Blöchl, Phys. Rev. B **50**, 17953 (1994).
[15] G. Kresse, Phys. Rev. B **59**, 1758 (1999).
[16] J. P. Perdew, K. Burke, and M. Ernzerhof, Phys. Rev. Lett. **78**, 1396 (1997).
[17] S. Grimme, J. Antony, S. Ehrlich, and S. Krieg, J. Chem. Phys. **132**, 154104 (2010).
[18] A. Togo and I. Tanaka, Scr. Mater. **108**, 1 (2015).
[19] M. Fishman, H. L. Zhuang, K. Mathew, W. Dirschka, and R. G. Hennig, Phys. Rev. B **87**, 245402 (2013).
[20] K. Mathew, R. Sundararaman, K. Letchworth-Weaver, T. A. Arias, and R. G. Hennig, J. Chem. Phys. **140**, 084106 (2014).
[21] R. Sundararaman and K. Schwarz, J. Chem. Phys. **146**, 084111 (2017).
[22] I. T. McCrum and M. J. Janik, J. Phys. Chem. C **120**, 457 (2016).
[23] K. A. Persson, B. Walsdwick, P. Lazic, and G. Ceder, Phys. Rev. B **85**, 235438 (2012).
[24] J. Kielland, J. Am. Chem. Soc. **59**, 1675 (1937).
[25] A. W. Adamson and A. P. Gast, *Physical Chemistry of Surfaces*, 6th ed. (A Wiley-Interscience Publication, New York, 1997), p. 606.